Optical Bio-sensing with an Asymmetric Hybrid Plasmonic Mach-Zehnder Interferometer

Optical Bio-sensing with an Asymmetric Hybrid Plasmonic Mach-Zehnder Interferometer

Souvik Ghosh* **and B M A Rahman**

School of Mathematics, Computer Science and Engineering (SMCSE), City, University of London, EC1V 0HB, United Kingdom.

*E-mail: souvik.ghosh.1@city.ac.uk

Abstract. A silicon (Si) suspended metal strip loaded hybrid plasmonic waveguide is designed and optimized to obtain a high waveguide sensitivity for bio-sensing applications. The waveguide forms a horizontal slot which confines a high ~59% power with the optimized design parameters. Any liquid refractometric changes can be detected by this waveguide and its quasi-TM waveguide sensitivity shows a very high value of >1. Finally, an asymmetric Mach-Zehnder interferometer (AMZI) is designed to detect a small refractometric change in terms of interferometric fringe shift. Our proposed design exhibits a high refractometric sensitivity of >400 nm/RIU. The AMZI is then considered to use for an accurate detection of haemoglobin (Hb) concentration of human whole blood. This ex vivo detection process exhibits a promising device sensitivity of -781.05 pm/g/dl with a detection limit of 1.3 mg/dl which makes this device useful for a precise detection of anaemic status of a patient.

1. Introduction

On-chip integrated plasmonic sensors have a great potential in applications for bio-medical industries, real-time rapid medical diagnosis, early-stage detection of critical diseases, DNA characterizations, environmental monitoring, food and water quality screening, pharmaceutical industries, particle tracing and tweezing [1]-[3]. Although several electronic and mechanical based sensors have already commercialized however users need to compromise with their bulky design, comparative lower detection accuracy, and high-power consumption. On the other hand, integrated optical sensors are more effective for its precise measurement and portable on- chip design thus could be considered as an alternative of electronic sensors. Remote operation, fast response, immunity from electromagnetic interference are other positive points of attraction of these photonic sensors.

Anaemia is one of the very common physiological disorder in which the number of oxygen carrying red blood cells (RBC) is insufficient to maintain normal physiological balance. This results in deficiency of body oxygen which in turn increase the risk of complications that affect the heart and lungs. More often iron deficiency considers as a common cause of anaemia or lower haemoglobin (Hb) concentrations. However, other nutritional deficiencies, bacterial and parasite infections, acute and chronic inflammation may also cause anaemia. Depending on human age, gender, pregnancy, and other external conditions the Hb concentrations have different ranges to classify the anaemic stages. Figure 1 shows the haemoglobin (Hb) levels of different anaemic and non-anaemic stages from the World Health Organization (WHO) report [4]. Nowadays, iron deficiency anaemia [5] is very common problem and its severity can be determined by screening the Hb concentration of patient blood.

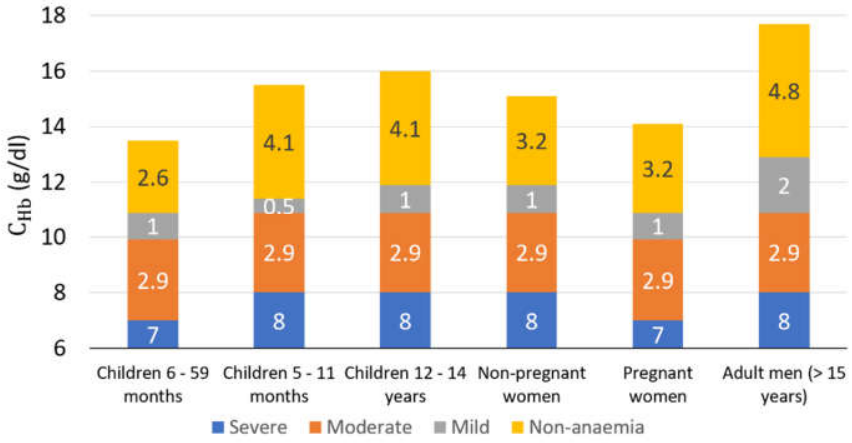

Figure 1. Haemoglobin (Hb) levels of different anaemic stages.

In this report we proposed a novel hybrid plasmonic waveguide design with a horizontal slot in between suspended silicon (Si) slab and deposited metal (Ag) layer on the silica (SiO_2) buffer layer. Main objective of the waveguide design is to enhance the power confinement in the horizontal slot region which results in a much higher and effective light-analyte interaction. Thus, a small refractometric change in the analyte could easily be tracked by the large change in waveguide effective index. Finally, an asymmetric Mach-Zehnder interferometer (AMZI) is designed for accurate measurement of the haemoglobin (Hb) concentration of the whole blood. The Ag metal strip loaded horizontal slot hybrid plasmonic waveguide (HSHPW) is used in the sensing arm and a SiO_2 clad $Si/SiO_2/Si$ dielectric horizontal slot (DHS) waveguide is used in the reference arm. This device is also susceptible to be used as an efficient bulk bio-chemical sensing and surface sensing applications. The device is designed and simulated with our in-house full-vectorial H - field based finite element method (FV-FEM) and the waveguide junction analyses have been simulated with the least squares boundary residual (LSBR) method.

2. Device design

2.1. Waveguide materials

The HSHPW consisting of silicon (Si), silica (SiO_2), and silver (Ag). As a detection bio-chemical liquid we have considered isopropanol solution of different concentrations. And finally, Hb- H_2O solution with different Hb concentration is used device design and performance analyses. Temperature and wavelength dependent Si and SiO_2 refractive indices are obtained from the Sellmeier equations in [6] and [7], respectively. The isopropanol refractive index is obtained from least-squares approximation based Sellmeier equation [8]. The wavelength dependent complex refractive index of the silver (Ag) metal is evaluated by the Drude model as

$$\epsilon(\lambda) = \epsilon_r + j\epsilon_i = \epsilon_\infty - \frac{\omega_p^2}{\omega(\omega + j\omega_c)} \quad (1)$$

where the ϵ_∞ and collision frequency (ω_c) are taken as 3.1 and 0.31×10^{14} rad/s, respectively. The plasma frequency (ω_p) is defined as,$\omega_p = \omega_{p0} \cdot e^{A_V(T_0)(T-T_0)/2}$ where ω_{p0}, A_V are the plasma frequency at the room temperature (T_0) and volume expansion coefficient ($A_V = 3A_L = 5.7 \times 10^{-5}$ /°C) of Ag, respectively.

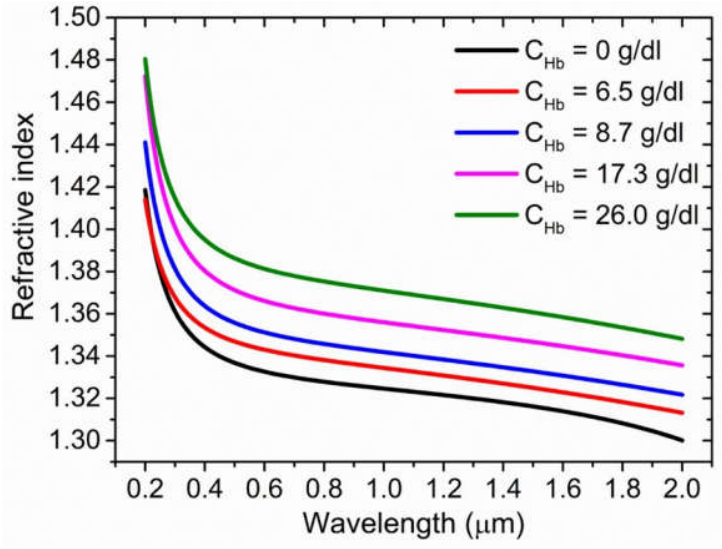

Figure 2. Refractive index variation of haemoglobin (Hb) solutions.

Lazareva *et al.* have experimentally measured the refractive index of Hb solution at four different Hb concentrations such as 6.5, 8.7, 17.3, and 26.0 g/dl [9]. The refractive index dispersion of the haemoglobin (Hb) solution at different Hb concentrations can also be obtained from the Sellmeier equation (Eq. 2) acceptable for the wavelength range of 0.2 μm to 2.0 μm shown in figure 2.

$$n_{Hb}(\lambda) = \sqrt{1 + \frac{A_1\lambda^2}{\lambda^2 - B_1} + \frac{A_2\lambda^2}{\lambda^2 - B_2}} \tag{2}$$

here the coefficients (A_1, B_1, A_2, and B_2) of the Sellemeier equation can be found in the following Table 1.

Table 1. Optical coefficients for different concentrations of Hb solutions.

Hb (g/dl)	$\boldsymbol{A_1}$	$\boldsymbol{B_1}$ $(\boldsymbol{\mu m^{-2}})$	$\boldsymbol{A_2}$	$\boldsymbol{B_2}$ $(\boldsymbol{\mu m^{-2}})$
6.5	0.79099	8.36645239×10^{-3}	685.08237	4.02435×10^{4}
8.7	0.80835	9.98369749×10^{-3}	450.24119	2.84283×10^{4}
17.3	0.84507	$11.06532117\times 10^{-3}$	402.89873	2.54072×10^{4}
26.0	0.88871	$10.18717167\times 10^{-3}$	190.95319	1.03998×10^{4}

2.2. Design and optimization of waveguides

The metal strip loaded horizontal slot hybrid plasmonic waveguide (HSHPW) supports a plasmon assisted slot confined hybrid mode in the low index slot area which is a combination of dielectric and plasmonic modes arise from dielectric-dielectric (Si/liquid) and dielectric-metal (liquid/Ag) interfaces, respectively. The HSHPW is placed in the sensing arm of the asymmetric Mach-Zehnder interferometer (AMZI) shown in the figure 3(a). The HSHPW is butt-coupled with SiO_2 clad Si/SiO_2/Si dielectric horizontal slot waveguides at both ends. Thus, the Si slab forms a suspended bridge over the deposited Ag layer and the gap in between Si slab and Ag layer forms a low index horizontal slot useful for both bulk and surface sensing applications. The cross-section of the HSHPW and DHS waveguide are shown in figure 3(a) and (b), respectively.

An accurate full-vectorial **H**-field based two-dimensional finite element method (FV-FEM) [10]-[13] is used for the waveguide modal solutions. Figures 4(a) and (b) represent the FV-FEM simulated quasi-TM E_y field distributions of the HSHPW and SiO_2 clad DHS waveguide. The 1D line plot of the E_y and H_x fields along y-axis of both the waveguides are shown in figure 4(c). The quasi-TM E_y field shows

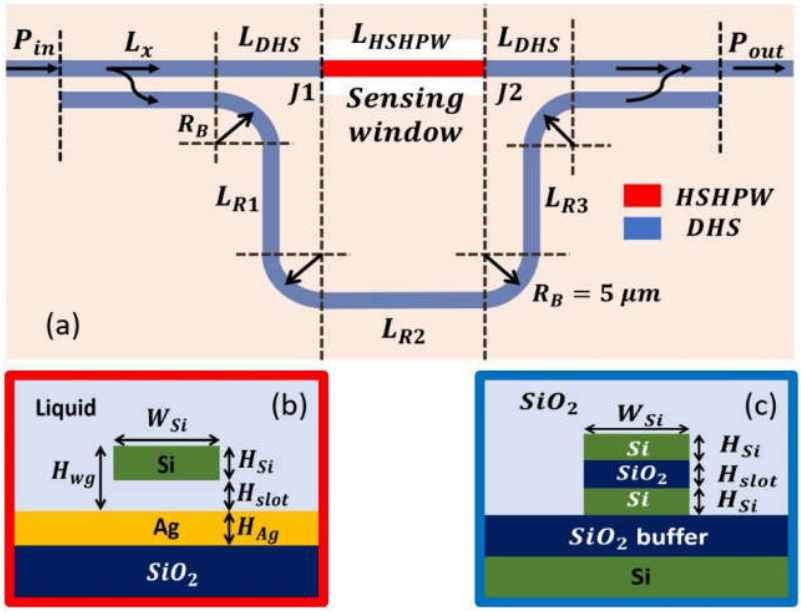

Figure 3. (a) Schematic diagram of the metal strip loaded HSHPW assisted AMZI. The HSHPW and DHS are employed at the sensing and the reference arms of the AMZI. (b) and (c) represent the cross-section of the metal (Ag) strip loaded HSHPW and SiO_2 clad DHS waveguide.

maximum light confinement in the low index slot region. E_y and H_x field profiles of HSHPW and DHS are matching closely which helps to reduce the butt-coupling loss at both the junctions ($J1$ and $J2$ in figure 3(a)). The HSHPW consists of a deposited thin metal layer on top of SiO_2 buffer. We considered the metal thickness as, H_{Ag}= 150 nm. Waveguide modal loss increases rapidly with the reduction of H_{Ag} from 150 nm. Thus, to match the dimensions of butt-coupled HSPW and DHS, we considered H_{Ag} and height of lower Si slab (H_{Si}) of DHS as 150 nm. It is also noticeable that in case of HSHPW, the Ag+SiO_2 buffer layer only confines a negligible ~0.1% light. Therefore, the guided light does not penetrate in the Ag metal and SiO_2 buffer layer rather mostly stays in the slot and sensing (slot + clad) region which on other way enhance the accessible field confinement into slot and sensing region.

An accurate design of sensing waveguide demands optimization of the light guiding parameters to confine the maximum light power in the sensing region. Figures 5(a) depicts the combined effect of W_{Si} and H_{Si} on the slot confinement Γ_{slot}. H_{Ag} and H_{slot} are kept fixed at 100 nm. The contour distribution of Γ_{slot} shows an intense light confinement of over 50% for the W_{Si} and H_{Si} within a range of 700 to 800 nm and 100 to 180 nm, respectively. More precisely, we have taken the optimized value of W_{Si} and H_{Si} as 740 nm and 150 nm, respectively to obtain a high Γ_{slot} = 59.24%. In figure 5(a) an abrupt Γ_{slot} variation is observed when W_{Si} > 800 nm and H_{Si} is in the range of 150 to 300 nm. This local change is due to the influence of second order quasi-TE mode (where more light confines in the Si slab) within a close proximity of the quasi-TM fundamental mode. Figures 5(b) and (c) show the quasi-TM and TE power confinements (Γ_{slot}, Γ_{clad}, and $\Gamma_{slot+clad}$) with H_{slot} when W_{Si}, H_{Si}, and H_{slot} are kept fixed at 740, 150, and 150 nm, respectively. The quasi-TM Γ_{slot} increases, reaches a maximum value of 59.38% at H_{slot} = 90 nm and then gradually decreases with the increment of H_{slot}. The Γ_{clad} increases with the H_{slot} (red dashed line) and shows a maximum power confinement of 22.80% for H_{slot} = 100 nm. Therefore, the resultant $\Gamma_{slot+clad}$ (blue dashed-dotted line) shows a bell-shaped variation with its peak at $\Gamma_{slot+clad}$ = 82.04% for 100 nm H_{slot}. Besides, figure 5(c) shows a similar variation with H_{slot} but for the fundamental quasi-TE mode.

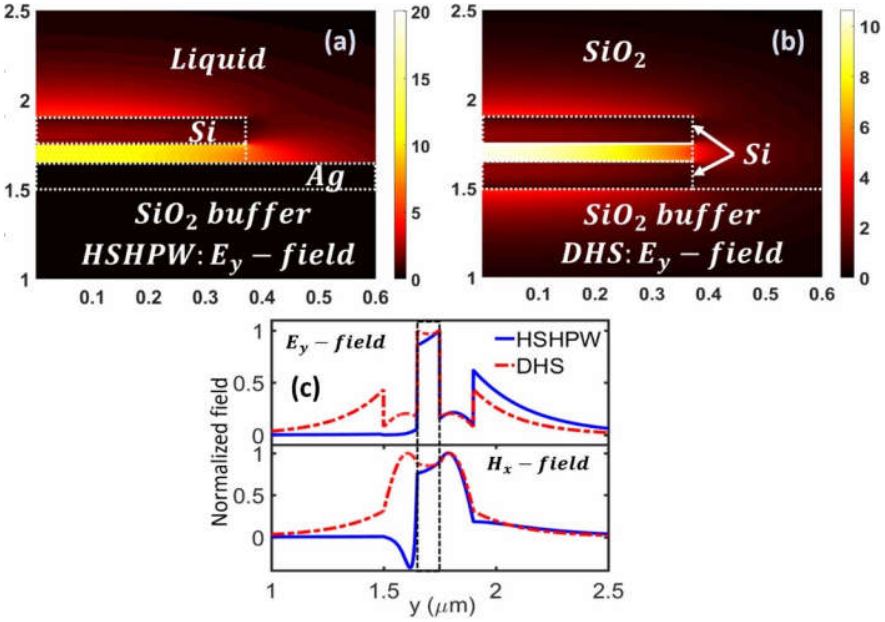

Figure 4. (a) and (b) show the 2D FV-FEM simulated quasi-TM E_y field distributions of the HSHPW and SiO_2 clad DHS waveguide. (c) exhibits the 1D E_y and H_x field line plots of both the waveguides along y-axis.

Within the complete range of H_{slot} (40 to 150 nm), the slot and clad region confine a much lower power (Γ_{slot} and Γ_{clad}) than that of the quasi-TM mode. Here the sensing region shows only ~30 to 34% power confinement ($\Gamma_{slot+clad}$) within the range of H_{slot}. The lower power confinement in the low index slot makes the quasi-TE mode less sensitive to the small refractometric changes of liquid.

In summary, fundamental quasi-TM mode is highly sensitive to slot refractometric changes and thus useful for sensing applications. Optimization of the waveguide design parameters result in a much higher slot and slot + clad confinements of 59.24% and 82.04%, respectively and modal attenuation (α'_{HSHPW}) of 0.036 dB/μm. Finally, the optimized HSHPW design parameters can be listed as, Si slab width (W_{Si}) = 740 nm, Si slab height (H_{Si}) = 150 nm, slot height (H_{slot}) = 100 nm and thickness of Ag strip (H_{Ag}) = 150 nm. On the other hand, SiO_2 clad DHS waveguide follows the dimensions of W_{Si} = 740 nm, H_{Si} = 150 nm, and H_{slot} = 100 nm.

2.3. Design of asymmetric Mach-Zehnder interferometer (AMZI)

An unbalanced, asymmetric Mach-Zehnder interferometer (AMZI) with unequal power spiller/combiner at the input and output is designed and used as transducer device in detection of small refractive changes of the sensing liquid. The complete on-chip schematic of the AMZI is shown in figure 3(a) where a HSHPW of length L_{HSHPW} is inserted in between fixed length SiO_2 clad DHS waveguides (L_{DHS} = 10 μm) at both ends, together they form the sensing arm of length, $L_{Sen} = 2L_{DHS} + L_{HSHPW}$. The reference arm consists of only SiO_2 clad DHS with four 90° bends of radius R_B = 5 μm and straight sections (L_{R1}, L_{R2}, and L_{R3}) to make the device feasible to change the arm length for calibration of frequency spectral range (FSR) and sensitivity (S_D). Thus, the reference arm length (L_{Ref}) can be calculated as, $L_{Ref} = (2\pi R_B) + L_{R1} + L_{R2} + L_{R3}$. The straight section, L_{R2} is considered to have same length as L_{HSHPW} in the sensing arm. The AMZI has SiO_2 cladding as cover medium except for HSHPW section which creates a sensing window, by which the sensing liquid could be infiltrated in the sensing region. During sensing process, the differential phase change ($\Delta\phi$) between both arms depends on the optical path difference (OPD) arises due to refractive index change of sensing liquid as

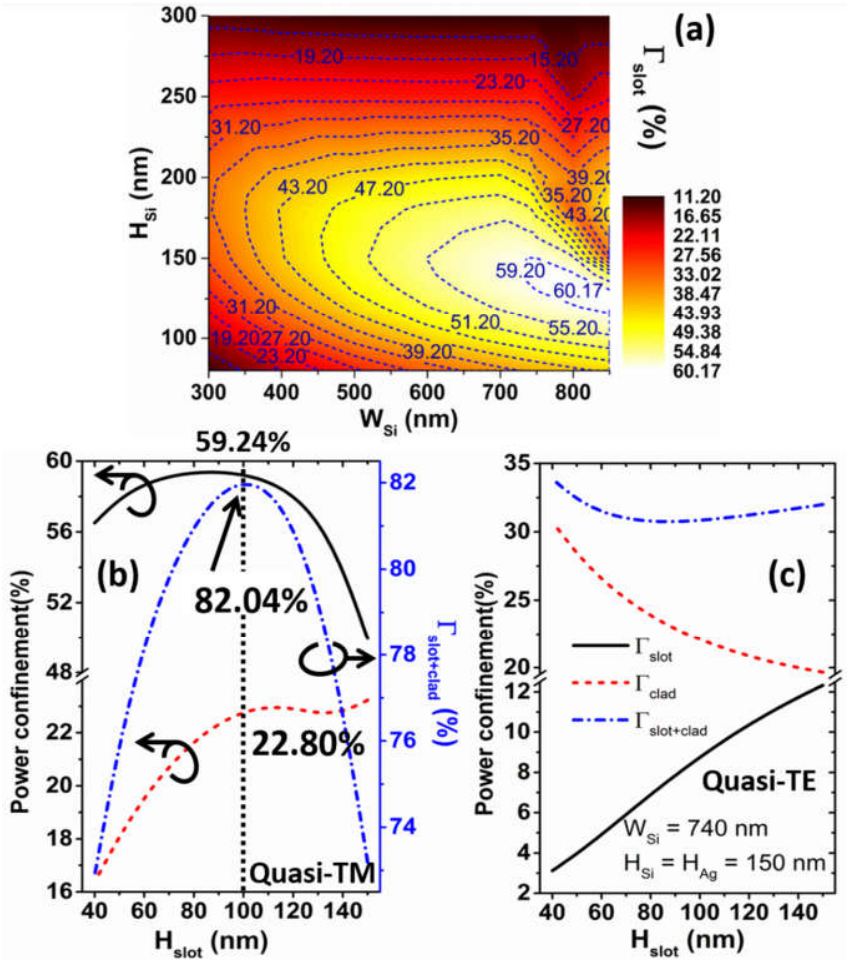

Figure 5. (a) shows the contour plot of the slot confinement (Γ_{slot}) depending on the width and height of the Si core. (b) and (c) present the power confinement variation in the slot and sensing (slot+clad) region for the quasi-TM and TE mode, respectively.

$$\Delta\phi = \frac{2\pi}{\lambda}\left[\left(n_{eff,DHS} \cdot 2L_{DHS} + n_{eff,HSHPW} \cdot L_{HSHPW}\right) - \left(n_{eff,DHS} \cdot L_{Ref}\right)\right] \quad (3)$$

where n_{eff} with subscripts HSHPW and DHS denote the real part of the effective indices of the respective waveguide. The HSHPW has a significant amount of quasi-TM modal loss whereas the DHS waveguide is considered to be loss-less due to its full dielectric configuration and considerably short length. Additionally, the butt-coupling losses at the sensing arm junctions $J1$ and $J2$ are also affect overall output power and interferometric fringe visibility (V). These losses and limitations could be compensated by tuning the coupling section (L_x) of the input directional coupler so that, the sensing arm receives more power to balance the device insertion loss and also improves the interferometric fringe visibility (V). Furthermore, the only unaccounted loss comes from the small attenuation perturbation ($\Delta\alpha_s$) in the sensing HSHPW during homogeneous refractometric changes of testing liquid. Therefore, the AMZI output power (P_{out}) can be expressed as

$$P_{out}(\lambda) = \frac{1}{2}\left[P_{inR} + \left(P_{inS} \cdot \tau_{J1} \cdot \tau_{J2} \cdot e^{-2(\alpha_{HSHPW} \pm \Delta\alpha_s)L_{HSHPW}}\right)\right](1 + V\,cos\Delta\phi) \quad (4)$$

here V denotes the fringe visibility which has a modified form as

$$V = \frac{2\left(P_{inR} \cdot P_{inS} \cdot \tau_{J1} \cdot \tau_{J2}\right)^{1/2} \cdot e^{-(\alpha_{HSHPW} \pm \Delta\alpha_s) L_{HSHPW}}}{P_{inR} + P_{inS} \cdot \tau_{J1} \cdot \tau_{J2} \cdot e^{-2(\alpha_{HSHPW} \pm \Delta\alpha_s) L_{HSHPW}}} \quad (5)$$

where P_{inR} and P_{inS} represent the input power at the reference and sensing arms, respectively. α_{HSHPW} denotes the HSHPW mode attenuation constant in Np/μm. τ_{J1} and τ_{J2} denote the transmittance at the waveguide junctions $J1$ and $J2$. These transmittance values are evaluated by using our in-house rigorous least squares boundary residual (LSBR) method [14] and the results show the transmittance coefficients at the waveguide discontinuities as, $\rho_{J1} = \rho_{J2}$ = 0.85. Therefore, the junction transmittance has the value of $\tau_{J1} = \tau_{J2} = |\rho|^2$ = 0.73. This indicates the junction insertion loss of 1.377 dB. For this design, we have considered L_{HSHPW} = 40 μm which makes total sensing arm length of $L_{Sen} = 2L_{DHS} + L_{HSHPW}$ = 60 μm. Therefore, the total transmittance of the sensing arm becomes $\tau_{Sen} = \tau_{J1} \cdot \tau_{J2} \cdot \tau_{HSHPW}$ = 0.38. To compensate these losses an unequal power splitter is considered at the input of the AMZI. The coupling section (L_x) could be adjusted depending on the power requirements at the sensing and reference arms. The required input power distribution ratio (P_{in-Sen}/P_{in-Ref}) at the sensing and reference arms for L_{HSHPW} = 40 μm is 72%/28%. The free spectral range (FSR) of the AMZI transmitted spectrum can be calculated as

$$FSR = \frac{\lambda^2}{\left[\left(n_{g,HSHPW} \cdot L_{HSHPW} + n_{g,DHS} \cdot L_{DHS}\right) - n_{g,DHS} \cdot L_{Ref}\right]} \quad (6)$$

where λ, $n_{g,HSHPW}$, and $n_{g,DHS}$ denote the operating wavelength and group index of the HSHPW and DHS waveguide, respectively. In this device configuration, we considered the FSR to be 15 nm. The

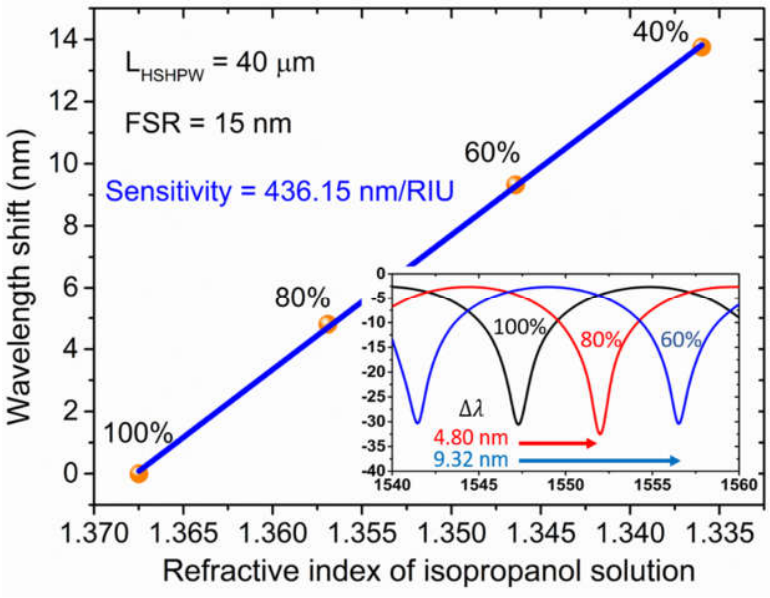

Figure 6. Variation of the spectral wavelength shift ($\Delta\lambda$) with the refractive index of isopropanol solution. Inset depicts the AMZI output spectra for different concentrations of isopropanol solution infiltrated in device sensing window. Black, red, and blue lines indicate the transmitted spectra for 100%, 80%, and 60% isopropanol solutions.

reference arm length (L_{Ref}) could be determined from Eq. 6 to maintain that FSR. Therefore, the reference arm length (L_{Ref}) will have the value of 116.4 μm to keep the FSR value fixed at 15 nm.

3. Results and analyses

Our target is to use the AMZI design for refractometric bulk sensing applications. First, the hybrid plasmonic waveguide incorporated AMZI is used for detection of refractive index differences that occur due to changes of liquid concentrations. Isopropanol solution of different concentrations are considered to be infiltrated in the sensing window of the AMZI. Inset of figure 6 shows the AMZI output power spectra for 100%, 80%, and 60% isopropanol solution shown by black, red, and blue lines, respectively. Different colored spectra for different concentrations show the red shift of the spectral peaks. These wavelength shifts ($\Delta\lambda$) are plotted against the refractive index variation of the isopropanol solutions of different concentrations in figure 6. Spectral wavelength shift exhibits a linear increment against liquid refractive index variations. Slope of this linear fitted curve denotes the device sensitivity for detection of refractive index changes as, $S_n = \Delta\lambda/\Delta n$. Thus, for the detection isopropanol volume concentration, the AMZI with L_{HSHPW} = 40 μm shows its sensitivity of 436.15 nm/RIU. The extinction ratio of the device has values larger than 20 dB.

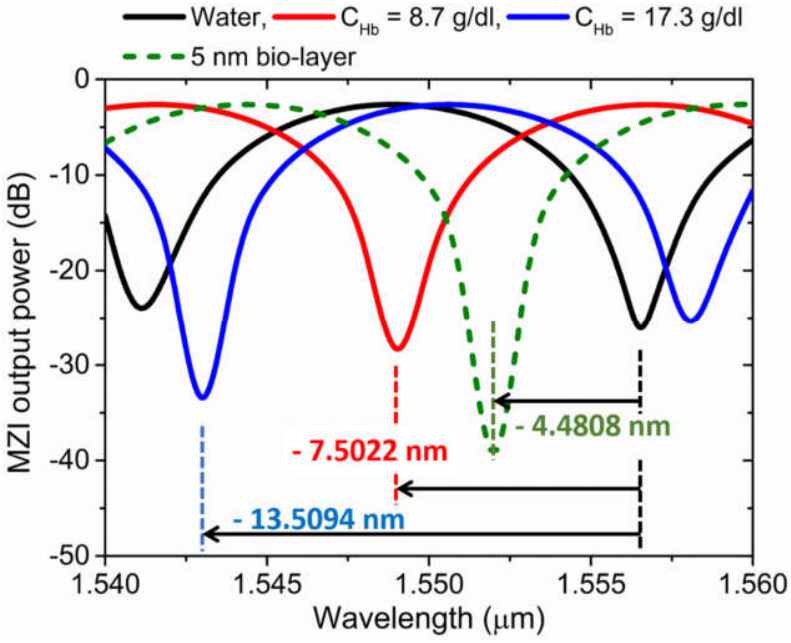

Figure 7. AMZI output spectra for different concentrations of Hb solutions. Black, red, and blue solid lines denote the output spectra for C_{Hb} = 0, 8.7, and 17.3 g/dl, respectively. The output spectrum of 5 nm bio-layer is shown by a green dashed line.

Next, haemoglobin (Hb) solution of different concentrations prepared from whole human blood are considered to be placed in the sensing region. The specimens with three different Hb concentrations (C_{Hb}) such as 0, 8.7, and 17.3 g/dl have considered here and the AMZI output power (P_{out}) spectra for those specific specimens are determined and plotted in figure 7. Black, red, and blue solid lines depict the transmitted spectra for 0, 8.7, and 17.3 g/dl Hb solutions, respectively. Here, 0 g/dl Hb solution i.e. distilled water is considered as the base solution and all the wavelength shift ($\Delta\lambda$) due to different Hb concentrations are evaluated from that. Refractive index of the Hb solution increases with the increment of Hb concentrations. Therefore, the output spectra of different Hb solutions show a blue shift. The spectrum of C_{Hb}= 8.7 and 17.3 g/dl show the spectral wavelength shift ($\Delta\lambda$) of -7.5022 nm and -13.5094

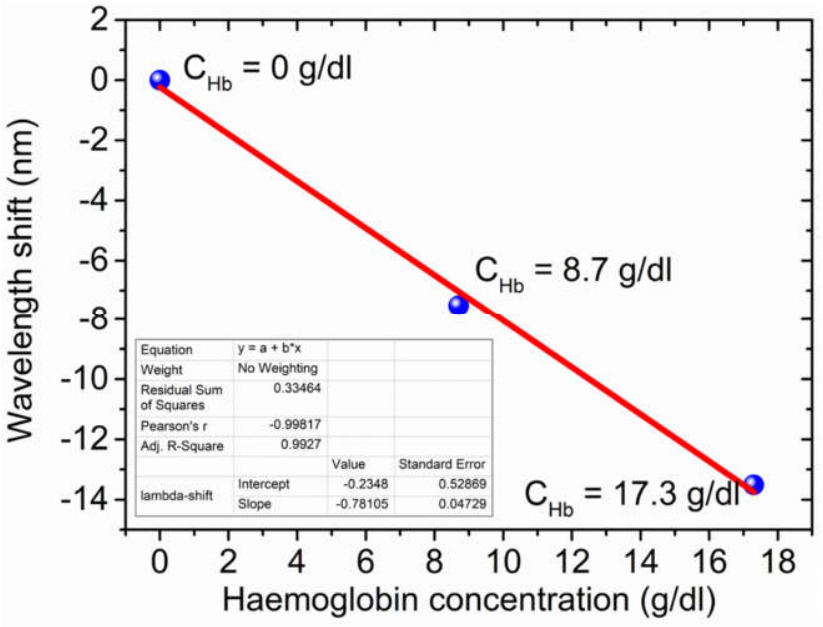

Figure 8. Variation of wavelength shift ($\Delta\lambda$) against concentration of Hb solution. The slope of the linear fitted curve indicates the AMZI sensitivity for the detection of Hb concentration.

nm, respectively from the base distilled water spectrum. These wavelength shifts ($\Delta\lambda$) are plotted against the C_{Hb} of the specimen shown in figure 8. A linear wavelength shift is observed. Slope of the linear fitted curve denotes the device sensitivity ($S_{Hb} = \Delta\lambda/\Delta C_{Hb}$) in detection of Hb concentration in the specimen extracted from the whole human blood. The result shows the AMZI sensitivity (S_{Hb}) of -781.05 pm/g/dl. On the other hand, detection limit is also an important parameter for a sensor. For our theoretical investigations, we have considered an approximate device resolution ($\lambda_{resolution}$) of 1 pm. Thus, the detection limit (DL_{Hb}) of the proposed AMZI for detection of Hb concentration is, DL_{Hb}= 0.0013 g/dl. This indicates that our proposed design could sense a very small Hb concentration change of ΔC_{Hb} = 1.3 mg/dl.

The AMZI is also efficient for surface sensing applications. An ultra-thin 5 nm bio-layer with refractive index of 1.45 is considered on the waveguide sensing region for our analysis. Presence of a 5 nm bio-layer results in a spectral shift of -4.48 nm, shown by a green dashed line in figure 7. Therefore, the device sensitivity for the surface sensing application shows a promising value of $S_{surface}$ = -896.15 pm/nm.

4. Conclusions

We report a novel design of metal strip loaded horizontal slot hybrid plasmonic waveguide (HSHPW) which is optimized for maximum power confinement in the horizontal slot section. Our in-house full-vectorial **H**-field based finite element method (FV-FEM) and least squares boundary residual (LSBR) method are used for design, optimization, and complete performance analyses of the device. The HSHPW shows a very high 59.24% and 82.04% power confinement in the horizontal slot and the sensing (slot + clad) region, respectively with a very low modal loss of 0.036 dB/μm. Considering a 40 μm long HSHPW in the sensing window, an asymmetric Mach-Zehnder interferometer (AMZI) is designed to have a 15 nm FSR. An unequal power slitter is also used to compensate the modal and junction losses. This also enhance the MZI fringe visibility (V) to its ideal value (V = 1). The complete AMZI is then used to sense the refractive index changes of the target liquid. A very high refractometric sensitivity of 436.15 nm/RIU is obtained. Finally, haemoglobin (Hb) solutions with different Hb concentrations are considered as the

testing liquid and a very high Hb sensitivity of -781.05 pm/g/dl is achieved with a detection limit of 1.3 mg/dl. Additionally, the AMZI has also shown an excellent result for surface sensing with a very high sensitivity of -896.15 pm/nm. These promising results indicate that the proposed on-chip design of asymmetric hybrid plasmonic Mach-Zehnder interferometer is highly capable in detection of Hb concentration. Thus, this photonic sensing device has a great potential in ex vivo detection of the anaemic stages of a patient.

Acknowledgements
This work was supported in part by City, University of London, UK and in part by Erasmus Mundus AREAS+ PhD fellowship and SPIE Optics and Photonics Education Scholarship 2017 program for PhD and research funding.

References
[1] V. M. N. Passaro, C. De Tullio, B. Troia, M. L. Notte, G. Giannoccaro, and F. De Leonardis, 2012 Recent advances in integrated photonic sensors, *Sens.* **12** 15558 –15598
[2] J. Homola, S. S. Yee, G. Gauglitz, 1999 Surface plasmon resonance sensors: review, *Sens. and Actuators B Chem.* **54** 3 – 15
[3] J. Homola 2003 Present and future of surface plasmon resonance biosensors *Anal. Bioanal. Chem.* **377** 528 – 539
[4] World Health Organization 2011 Haemoglobin concentrations for the diagnosis of anaemia and assessment of severity **WHO/NMH/NHD/MNM/11.1**
[5] A. Lopez, P. Cacoub, I. C. Macdougall, and L. P-Biroulet 2016 Iron deficiency anaemia *The Lancet* **387**(10021) 907 – 916
[6] H. H. Li 1980 Refractive index of silicon and germanium and its wavelength and temperature derivatives *J. Phys. Chem. Ref. Data* **9** 561 – 658
[7] I. H. Malitson 1965 Interspecimen comparison of the refractive index of fused silica *J. Opt. Soc. Am.* **55** 1205– 1208
[8] E. Sani and A. Dell'Oro 2016 Spectral optical constants of ethanol and isoprpanol from ultraviolet to far infrared *Opt. Mater.* **60** 137 – 141
[9] E. N. Lazareva and V. V. Tuchin 2018 Measurement of refractive index of hemoglobin in the visible/NIR spectral range *J. Biomed. Opt.* **23**(3) 035004
[10] B. M. A. Rahman and J. B. Davies 1984 Finite-element solution of integrated optical devices *J. Lightwave Technol.* **2** 682 – 688
[11] S. Ghosh and B. M. A. Rahman 2017 A compact Mach-Zehnder interferometer using composite plasmonic waveguide for ethanol vapor sensing *J. Lightwave Technol.* **35** 3003 – 3011
[12] S. Ghosh and B. M. A. Rahman 2018 Evolution of plasmonic modes in a metal nano-wire studied by a modified finite element method *J. Lightwave Technol.* **36** 809 – 818
[13] S. Ghosh and B. M. A. Rahman 2016 Full vectorial finite element modelling: a composite plasmonic horizontal slot waveguide as a bio-sensor, in: *13th International Conference on Fiber Optics and Photonics* Tech. Digest OSA paper Tu5C.3
[14] B. M. A. Rahman and J. B. Davies 1988 Analysis of optical waveguide discontinuities *J. Lightwave Technol.* **6** 52 – 57